Acidity of Sulfonic and Phosphonic Acid-Functionalized SBA-15 under Almost Water-Free Conditions

D. Mauder,[†] D. Akcakayiran,[§] S. B. Lesnichin,[†,‡] G. H. Findenegg,[§] and I. G. Shenderovich*[,†,‡]

Institut für Chemie und Biochemie, Freie Universität Berlin, Takustrasse 3, 14195 Berlin, Germany, Institut für Chemie, Technische Universität Berlin, Strasse des 17. Juni 124, 10623 Berlin, Germany, and Department of Physics, St. Petersburg State University, Ulianovskaya 1, 198504 St. Petersburg, Russian Federation

Received: July 24, 2009; Revised Manuscript Received: September 21, 2009

The hydrogen bond interaction of pyridine with sulfonic and phosphonic acid moieties at the surface of SBA-15 ordered mesoporous silica has been studied by a combination of solid-state NMR techniques. The composition of the materials is characterized by ^{29}Si MAS NMR, the residual water content is inspected by ^{1}H MAS NMR, and the hydrogen bond interactions are characterized by ^{15}N CPMAS NMR at 130 K using pyridine-^{15}N as a probe molecule. It is shown that (i) all acid moieties at the surface are accessible for pyridine; (ii) each sulfonic acid moiety interacts with one pyridine molecule; (iii) each phosphonic acid moiety can interact simultaneously with two pyridine molecules; (iv) for both materials the interaction of the acid moieties with the base results in proton transfer to pyridine. The observed proton-donating ability of the acid moieties depends on the presence of residual water. In contrast to nonfunctionalized SBA-15, the sulfonic acid-functionalized SBA-15 material contains about six water molecules per acid moiety after drying at 420 K in high vacuum. From the ^{15}N chemical shift of pyridine in the hydrogen-bonded complex, it is estimated that the proton-donating ability of the acidic functional groups solvated by such small water clusters is equivalent to that of acids in water exhibiting a pK_a of about 0.6 and 1.3, respectively, for the sulfonic and phosphonic acid moieties. The O···H and H···N distances in the hydrogen bond of the pyridine complex are $r_{OH} \approx 1.69$ Å and $r_{HN} \approx 1.05$ Å for sulfonic acid, as compared to $r_{OH} \approx 1.53$ Å and $r_{HN} \approx 1.09$ Å for phosphonic acid.

1. Introduction

It is well-known that the structure of proton donor−acceptor complexes is strongly dependent on their environment. The complex formed by hydrogen chloride and ammonia is a prototypical acid−base pair to demonstrate this effect. In the aqueous solution these species form a solvated ion pair, NH_4^+(aq) and Cl^-(aq). In contrast, in the gas phase they form a hydrogen-bonded complex without proton transfer, $H_3N\cdots HCl$, as evidenced by experiment[1,2] and theory.[3,4] Either the presence of an electric field[5] or other hydrogen bonds[6] is needed to stabilize the $H_3NH^+\cdots Cl^-$ structure. At least two water molecules are needed to promote proton transfer into $(H_4N^+\cdots Cl^-)\cdots(H_2O)_n$ clusters in the gas phase.[4] The effect of electric fields on the proton position in the $H_3N\cdots HCl$ complex was studied experimentally in argon and nitrogen matrices.[7] An increase of the matrix polarity results in a gradual proton shift toward ammonia. The same trends have been found in many other systems: they form solvated ion pairs, $[B-H]^+$ and A^-, in aqueous solutions; they form hydrogen-bonded complexes without proton transfer, B···H−A, in the gas phase; and they have solvent field dependent geometries, B···H···A, in aprotic solutions.[8−11] Electric field effects and coupled hydrogen bonds also affect the interaction of proton donor and acceptor groups in solids. In crystals these effects can often be evaluated due to the well-defined geometries. In contrast, for amorphous solids that are probably the most relevant materials for practical applications, one can rarely predict possible hydrogen bond networks or the presence of residual water. To describe the protonation state of proton donor and acceptor groups in a certain material, it has to be treated under well-defined conditions and inspected in detail. This problem is well-known for polymers.[12−15] A characterization of the proton-donating ability of highly ordered mesoporous silica materials is another challenging task. Because of their wide pore openings, narrow pore size distribution, large internal surface area, and tunable shape, ordered mesoporous silicas such as SBA-15, MCM-41, and MCM-48 have a high potential as catalytic supports and host materials for organic guest molecules and transition metals.[16−23] NMR studies of pure SBA-15 silica have shown that evacuation of the samples at 400 K for several hours is sufficient to remove adsorbed water and that the proton-donating ability of silanol groups is equivalent to that of acids of p$K_a \approx 5$ in water.[24,25] It was also found that in pure SBA-15 most of the surface silanol groups are isolated from each other. As a result, in the absence of water the pore walls of SBA-15 are relatively inert with regard to chemical reactions with guest molecules. For example, pyridine (Pyr) adsorption leads to the formation of hydrogen bonds Pyr···HO−Si, characterized by a N···H distance of about 1.7 Å.[24] The geometry of this bond is comparable to that of hydrogen bonds formed between pyridine and water molecules.[26]

Many applications of silica materials rely on a chemical modification of their surfaces by functional groups with task-oriented properties.[27−33] Structural aspects of such surface modification have been described recently.[25] The goal of the present study is to characterize the proton-donating ability of potentially strongly acidic functional groups on the surface of highly ordered SBA-15 silica under water-free conditions. We

* To whom correspondence should be addressed. E-mail: shender@chemie.fu-berlin.de.
[†] Freie Universität Berlin.
[‡] St. Petersburg State University.
[§] Technische Universität Berlin.

10.1021/jp907058y CCC: $40.75
Published on Web 10/09/2009

expect that the inspection of the properties of host−guest interactions will make it possible to characterize the environment of the functional groups attached to the surface. Indeed, Glezakou et al.[12] recently reported that in the gas phase the proton-donating ability of sulfonic acid is similar to the proton-donating ability of water. Mbaraka and Shanks[34] found that the pK_a value of sulfonic groups grafted onto silica is about 1 in the presence of methanol, and in samples exposed to ambient conditions the acidity of these functional groups is sufficient to protonate guest molecules.[35] Theoretical calculations support this finding, indicating that at least three water molecules are needed to stabilize deprotonated sulfonic groups.[12,36] At the same time, results of differential thermoanalysis (DTA) suggest that water is released from SBA-15 silica functionalized with sulfonic groups when heated to above 380 K.[34] This temperature is too low to cause any morphological changes in the material. Thus, evacuation at 420 K should render water-free (or at least almost water-free) silica host materials.

In the present work, we study the proton-donating ability of sulfonic ($R-SO_2OH$) and phosphonic groups ($R-PO(OH)_2$) attached by direct Si−C bonds to the surface of highly ordered SBA-15 silica that was evacuated overnight at 420 K. For this purpose, three types of measurements were necessary: (i) characterization of the composition of the materials using ^{29}Si MAS NMR, (ii) analysis of the water content after drying using ^{1}H MAS NMR, and (iii) study of acid−base interactions on the functionalized surfaces using ^{15}N CP MAS NMR at 130 K, using pyridine-^{15}N as the probe molecule.

2. Experimental Section

Three different SBA-15 mesoporous silica materials were used in this work: pure SBA-15, the sulfonic acid-functionalized material SBA-SA, and the phosphonic acid-functionalized material SBA-PA.

2.1. Materials. The SBA-15 silica materials used in this work were synthesized by the co-condensation method, using the following molar composition of the reagents[37]

$$(1-x)\text{TEOS}:x \text{ functional silane}:5.8\ \text{HCl}:193\ \text{H}_2\text{O}:0.017\ \text{P123}$$

where $x = 0$ for SBA-15, $x = 0.2$ for SBA-SA, and $x = 0.15$ for SBA-PA.

Pure SBA-15. Starting from a micellar hydrochloric acid solution of block copolymer P123, the appropriate amount of TEOS was added slowly under vigorous stirring at 40 °C. The polymer−silica composite, formed as a fine precipitate, was kept in the reaction solution at 40 °C for 20 h under continued stirring. The bottle with the reaction products was then transferred into an autoclave for aging at 90 °C for 24 h. After filtration and washing of the white precipitate, as-synthesized SBA-15 silica was obtained.

Sulfonic Acid-Functionalized SBA-15 (SBA-SA). For the synthesis of SBA-SA materials by the co-condensation route, the functional silane 3-(trihydroxysilyl)-1-propanesulfonic acid, STHS (30−35% in water, ABCR), was used. Starting from a micellar hydrochloric acid solution of block copolymer P123, the functional silane was added first under stirring at 40 °C. After a precondensation time (60 min), the respective amount of TEOS was added under continued stirring. The subsequent procedure was as in the case of pure SBA-15, leading to as-synthesized SBA-SA.

Phosphonic Acid-Functionalized SBA-15 (SBA-PA). For the synthesis of SBA-PA by the co-condensation route, (diethoxyphosphorylethyl)triethoxysilane, PTES (95%, ABCR), was chosen as functional silane. Starting from the micellar hydrochloric acid solution of block copolymer P123, the predetermined amount of TEOS was added at 40 °C under vigorous stirring. After 40 min prehydrolysis time, the respective amount of PTES was added, and the precipitate was kept in the reaction solution for 20 h at 40 °C under continued stirring. The bottle with the reaction products was then transferred into an autoclave for aging at 100 °C for 24 h. After filtration and washing, as-synthesized SBA-PA was obtained.

TABLE 1: Pure SBA-15 and Acid-Functionalized SBA-15 Mesoporous Silica Materials Studied in This Work[a]

sample	a_s/m^2 g^{-1}	v_p/cm^3 g^{-1}	D/nm	a_0/nm
SBA-15	810	1.35	10.2	12.5
SBA-SA	560	0.94	9.8	12.9
SBA-PA	530	0.66	7.5	12.0

[a] a_s, BET specific surface area; v_p, specific mesopore volume; D, mean pore diameter from the adsorption branch of the nitrogen isotherm; a_0, lattice parameter from SAXD measurements.

Polymer Removal. The as-synthesized silica materials were treated with 48% aqueous sulfuric acid to remove the template and produce the final products. Typically, 1 g of as-synthesized SBA-15 was suspended in 200 mL of 48% H_2SO_4 solution and refluxed under stirring at 95 °C for 24 h. After filtration the powders were washed extensively, first with acetone and ethanol and then with water until the pH of the eluent was neutral. Finally the product was dried at 60 °C.

Cleavage of Phosphonate Ester Groups. In the case of SBA-PA, it turned out that refluxing of the as-synthesized product with 48% H_2SO_4 at 95 °C during the polymer removal step was not enough for complete dealkylation of the phosphonate ester groups to produce the free phosphonic acid functionality. To complete the cleavage of phosphonate ester, the sample was fluxed in concentrated HCl. For this purpose, ca. 1 g of the H_2SO_4 treated material was suspended in 300 mL of 37% HCl and refluxed under stirring at 95 °C for 24 h. After filtration the powder was washed extensively with water until the eluent was pH neutral.

Characterization. The pure and acid-functionalized silicas were characterized by nitrogen adsorption, small-angle X-ray diffraction (SAXD), and scanning electron microscopy (SEM). Nitrogen adsorption isotherms (77 K) were measured by gas volumetry using a Gemini 2375 volumetric gas adsorption analyzer (Micromeritics). SAXD profiles were recorded in a range of the scattering vector q from 0.3 to 2 nm^{-1} by a Bruker SAXS Nanostar machine, using a 2D HI Star area detector and Cu Kα radiation ($\lambda = 1.54$ Å). Details of the nitrogen adsorption and SAXD measurements are presented elsewhere.[38−40] Resulting values of the specific surface area a_s, pore volume v_p, mean pore diameter D (determined from the pore condensation pressure by the improved KJS method[40]), and lattice parameter a_0 are given in Table 1. Nitrogen adsorption isotherms and SAXD profiles for the three silica materials and SEM pictures of SBA-SA and SBA-PA silica are shown in the Supporting Information of this work.

Synthesis of Pyridine-^{15}N. The pyridine-^{15}N (about 98% ^{15}N-enriched) used in this study was synthesized in our lab following the procedure described by Whaley and Ott.[41] To keep it water-free, it was stored over dried molecular sieve (4 Å).

Sample Preparation. The pure and acid-functionalized SBA-15 samples used for ^{15}N CPMAS NMR experiments were prepared as follows. The silica material was placed into a 6 mm pencil NMR rotor equipped with a Teflon insert and a

special cap appropriate for low-temperature measurements. The samples were then dried in the open rotor in high vacuum (10^{-5} mbar) overnight (>18 h) at 420 K. ^{1}H NMR spectra were measured immediately after closing the rotor. Pyridine-^{15}N was added to the silica inside the rotor with a micropipet under nitrogen atmosphere in a glovebag to avoid water uptake. The pyridine-to-silica mass ratio of the different samples is given below in Table 3. After a waiting time of at least 6 h, which allows pyridine to be distributed uniformly in the pores of the silica, low-temperature ^{15}N CPMAS NMR spectra were measured.

2.2. NMR Measurements. ***^{29}Si and ^{13}C NMR Measurements.*** ^{29}Si and ^{13}C NMR measurements were performed on a Bruker MSL-300 instrument operating at 7 T and equipped with a Chemagnetics-Varian 6 mm pencil CPMAS probe. All samples were spun at 6 kHz under magic angle spinning (MAS) conditions. The ^{29}Si MAS spectra were recorded employing a $\pi/12$ pulse sequence, a recycle delay of 180 s, and 800 scans. The ^{13}C NMR measurements were performed employing the $\{^1H\}-^{13}C$ CPMAS technique with a CP contact time of 2 ms and a recycle delay of 5 s. The ^{13}C and ^{29}Si chemical shift values are referenced to solid TSP ((trimethylsilyl)propionic acid sodium salt).

The ^{13}C CPMAS NMR spectra are shown in the Supporting Information of this work.

^{1}H NMR Measurements. The ^{1}H NMR measurements were performed on a Bruker MSL-300 instrument operating at 7 T, equipped with a variable-temperature Chemagnetics-Varian 6 mm pencil CPMAS probe. The samples were spun at 6−8 kHz under MAS conditions. The ^{1}H MAS spectra were recorded employing a $\pi/2$ pulse sequence, with a 90° pulse length of 3.5 μs and a recycle delay of 5 s. The number of scans was 16−64. All ^{1}H chemical shift values are referenced to solid TSP.

^{15}N NMR Measurements. The ^{15}N NMR measurements were performed on a Bruker MSL-300 instrument operating at 7 T, equipped with a variable-temperature Chemagnetics-Varian 6 mm pencil CPMAS probe. The samples were spun at 6−8 kHz under MAS conditions. The $\{^1H\}-^{15}N$ CPMAS spectra were recorded using a cross-polarization contact time of 5 ms, and the typical 90° pulse lengths were about 4.0 μs. The number of scans was 512−2048. The measurements were performed at 130 K. All ^{15}N chemical shift values are referenced to pyridine-^{15}N and can be converted into the solid $^{15}NH_4Cl$ scale by the relation $\delta(^{15}NH_4Cl, \text{solid}) = \delta(\text{pyridine-}^{15}N, \text{frozen}) + 275.5$ ppm.

2.3. Geometric and NMR Hydrogen Bond Correlations. In earlier studies it was shown that the isotropic ^{15}N chemical shift of pyridines can be used to estimate the H···N distance in hydrogen-bonded complexes with these heterocycles.[24,26,42] The method is based on a correlation between the distances r_{OH} and r_{HN} of OHN hydrogen bonds[43]

$$p_{OH} + p_{HN} = 1; \quad p_{OH} = \exp\{-(r_{OH} - r^0_{OH})/b_{OH}\}; \quad p_{HN} = \exp\{-(r_{HN} - r^0_{HN})/b_{HN}\} \quad (1)$$

where p_{OH} and p_{HN} represent the Pauling valence bond orders, and $r^0_{OH} = 0.942$ Å, $r^0_{HN} = 0.992$ Å, $b_{OH} = 0.371$ Å, and $b_{HN} = 0.385$ Å are empirical parameters derived by analysis of a series of neutron structures. For complexes involving pyridines, a better fit was found when using $b_{HN} = 0.42$ Å,[42] and this value of b_{HN} was adopted in the present work. We found the following expression for the isotropic ^{15}N chemical shift $\delta(^{15}N)$ as a function of the bond order p_{HN}

$$\delta(^{15}N) = \delta^{\infty}_{HN} - (\delta^{\infty}_{HN} - \delta^{0}_{HN})\cdot p_{HN} \quad (2)$$

In this equation, $\delta^{\infty}_{HN} = 0$ ppm is the isotropic ^{15}N chemical shift for non-hydrogen-bonded pyridine, and $\delta^{0}_{HN} = -126$ ppm is the limiting isotropic ^{15}N chemical shift for protonated pyridine. Recently these empirical correlations were modified.[44] However, these modifications are important only for quasi-symmetric hydrogen bonds and are neglected here. In ref 42 a dependence of the geometry of solid-state acid−pyridine complexes on the pK_a values of the acids was deduced and formulated as follows

$$pK_a = -3.5\cdot(r_{OH} - r_{HN}) + 2.8 \quad (3)$$

However, in the present context, the reference to a pK_a scale is of limited significance. It only means that the length of the H···N hydrogen bond is the same as in a crystalline complex with a carboxylic acid exhibiting in water the corresponding pK_a value.

3. Results

In this section the results of the solid-state NMR experiments are reported. Pure SBA-15 and the functionalized materials SBA-SA and SBA-PA were characterized by the following measurements: (i) ^{29}Si MAS NMR to get information about the degree of surface functionalization, (ii) ^{13}C CPMAS NMR to prove the removal of the structure-directing template material after synthesis and the presence of the introduced functional groups, (iii) ^{1}H MAS NMR before and after silica drying to monitor water presence in samples, and (iv) ^{15}N CPMAS NMR measurements at 130 K of pyridine-^{15}N loaded materials to characterize the proton-donating ability of the functional groups and the structure of hydrogen-bonded complexes formed between these groups and pyridine. The symbols Q^n and T^m used to specify the different types of silicon atoms in these samples are explained in Scheme 1.

3.1. ^{29}Si MAS NMR. ^{29}Si MAS NMR spectra of the samples SBA-15, SBA-PA, and SBA-SA are presented in Figure 1.

The spectra exhibit two main regions of peaks, denoted as T^m and Q^n ($m = 1, 2, 3$; $n = 1, 2, 3, 4$), where T^m represents (**Si**$(OSi)_m(OH)_{3-m}R$) and Q^n represents (**Si**$(OSi)_n(OH)_{4-n}$) structures (see Scheme 1). Silicate groups of the silica lattice (Q^4) resonate at −112 ppm and surface silanol groups (Q^3) at −102 ppm. The Q^3:Q^4 ratio for the nonfunctionalized material is about 1:2.5. For SBA-SA, both T^3 (at −66 ppm) and T^2 (at −58 ppm) groups can be identified. In contrast, for SBA-PA one observes T^3 (at −66 ppm) but no T^2 groups. The degree of surface functionalization with sulfonic and phosphonic acid moieties can be expressed in terms of the mole fraction of the functional groups, x_{FG}, which is calculated from the integrated intensities of the corresponding signals as $x_{FG} = N_{FG}/(N_{Q^3} + N_{FG}) = (T^2 + T^3)/(Q^3 + T^2 + T^3)$. Here, N_{FG} is the number of silicon atoms carrying a functional group, and N_{Q^3} is the number of Q^3 silanol groups. The number of Q^2 groups is small and is neglected in the calculation. The degree of functionalization determined in this way is 25% for SBA-SA and 36% for SBA-PA. In addition, it is of interest to calculate the ratio $N^{acid}_{OH}/N^{silanol}_{OH}$, where N^{acid}_{OH} is the number of acidic hydroxyl groups (one for each sulfonic acid moiety and two for each phosphonic acid moiety), and $N^{silanol}_{OH}$ is the number of silanol groups of Q^3 and T^2 type. For SBA-SA we have $N^{acid}_{OH}/N^{silanol}_{OH} = (T^3 + T^2)/(Q^3 + T^2)$, while for SBA-PA $N^{acid}_{OH}/N^{silanol}_{OH} = (2\cdot T^3)/Q^3$, because no T^2 signal was detectable in this case. Results for the integrated signal intensities

SCHEME 1: Schematic Representation of the Different Silica Species in (a) SBA-15, (b) SBA-SA, and (c) SBA-PA Material, Detected by ^{29}Si MAS NMR

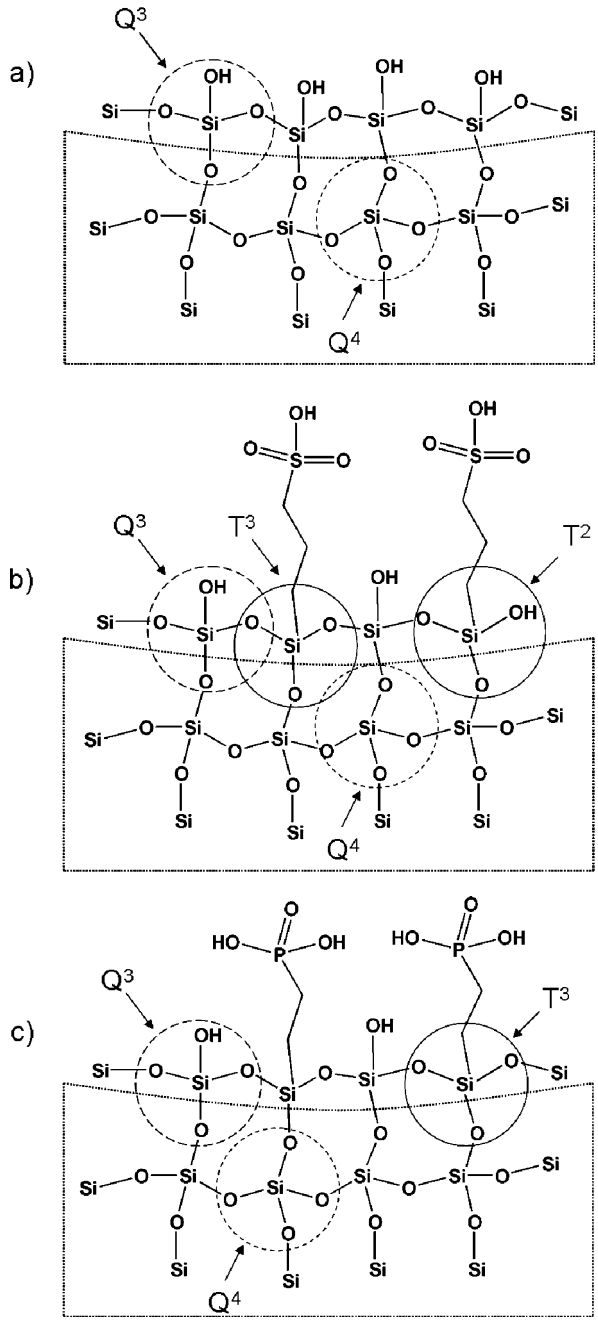

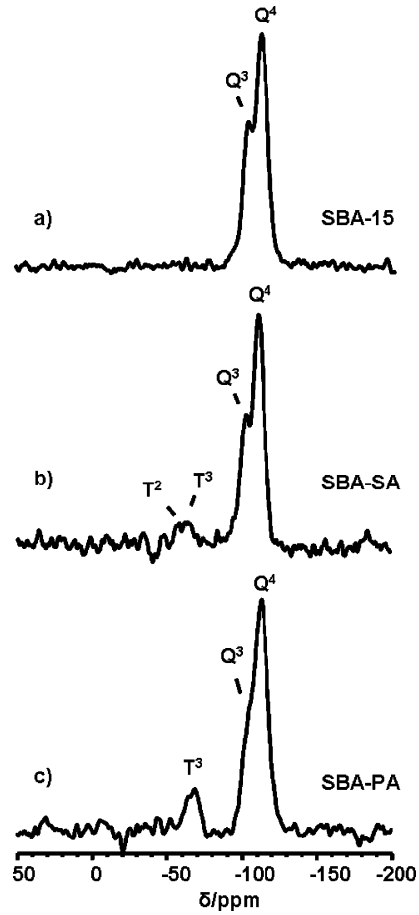

Figure 1. Solid-state ^{29}Si MAS NMR spectra of (a) SBA-15; (b) SBA-SA; (c) SBA-PA.

TABLE 2: Relative Integrated Intensities of Different Signals in ^{29}Si MAS NMR Spectra of SBA-15, SBA-SA, and SBA-PA Materials[a]

sample	T^2	T^3	Q^3	Q^4	x_{FG}	$N_{OH}^{acid}/N_{OH}^{silanol}$
SBA-15	–	–	41	100	–	–
SBA-SA	5	9	43	100	0.25	0.29 (0.33)
SBA-PA	–	21	37	100	0.36	1.14[b]

[a] x_{FG}, mole fraction of functional groups; $N_{OH}^{acid}/N_{OH}^{silanol}$, ratio between hydroxyl groups of a different acidity ("effective" value is given in parentheses). See text for detailed explanations. [b] It is taken into account that each phosphonic acid fragment carries two hydroxyl groups.

from spectra deconvolution, and the corresponding values of x_{FG} and $N_{OH}^{acid}/N_{OH}^{silanol}$, are collected in Table 2.

3.2. ^{13}C CPMAS NMR. As explained in section 2.1, template removal from the as-synthesized composite samples was performed not by calcinations but by treatment with sulfuric acid, in order to avoid thermal decomposition of the organic groups in the functionalized silicas. ^{13}C CPMAS NMR is the most appropriate tool to detect the presence of the functional groups and the removal of the template.[45,46] ^{13}C CPMAS NMR spectra of SBA-SA and SBA-PA prove the presence of $-(CH_2)_n-$ chains of the functional groups and the complete removal of the block copolymer template. For details see the Supporting Information.

3.3. ^{1}H MAS NMR. At ambient conditions mesoporous silica materials contain some adsorbed water, which interacts with the silanol groups. At higher loadings a second and further adsorbed layers and/or bulklike water in the core of the pore space can be formed. As a result, there are different resonances in ^{1}H MAS NMR spectra of mesoporous silicas whose characteristics depend on the water content.[47−49] The ^{1}H MAS NMR spectrum of the pure SBA-15 sample exposed to ambient conditions is depicted in Figure 2a. Its spectral pattern resembles a spectrum of calcined SBA-15 silica containing eight water molecules per nm^2.[47] Evacuation of this pure silica sample at 420 K causes complete removal of the adsorbed water. This is indicated by the fact that the only remaining resonance at 1.8 ppm is a fingerprint of isolated silanol groups (Figure 2b).[24] The functionalized materials, SBA-SA and SBA-PA, exposed to ambient conditions also contain a remarkable amount of adsorbed water (Figures 2c and 2e). Evacuation of these samples overnight at 420 K again results in a strong decrease of the amount of water (Figures 2d and 2f). However, the spectrum of evacuated SBA-PA contains two peaks. The peak centered

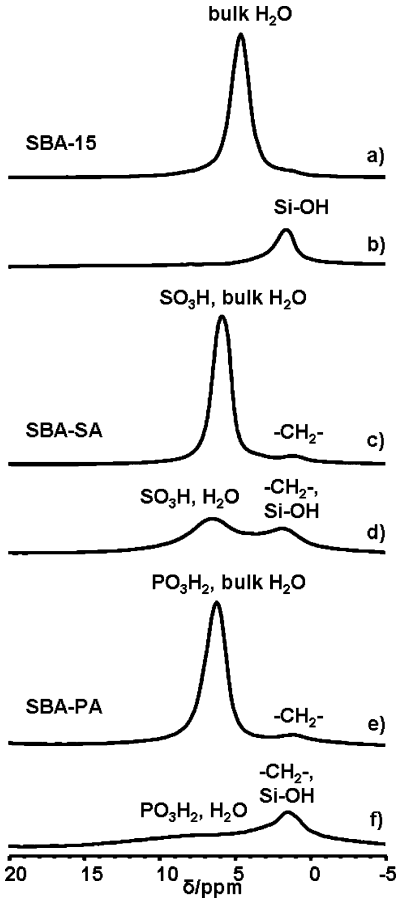

Figure 2. ^{1}H MAS solid-state NMR spectra at room temperature of different silica samples before (upper) and after (lower) drying procedure. (a), (b) SBA-15; (c), (d) SBA-SA; (e), (f) SBA-PA.

at 1.5 ppm can be attributed to overlapping resonances of $-(CH_2)_2-$ chains and isolated silanols, while a further very broad peak covering the region down to 15 ppm is assigned tentatively to protons of the phosphonic acid interacting with residual water.[35,50,51] The spectrum of SBA-SA also shows two peaks centered at 1.8 and 6.5 ppm. The ratio of their integrated intensities is about 2:3. The assignment of the resonances is the same as for SBA-PA.

3.4. ^{15}N CPMAS NMR of Samples Containing Pyridine-^{15}N. To evaluate the proton-donating ability of sulfonic ($R-SO_2OH$) and phosphonic ($R-PO(OH)_2$) groups at the surface of SBA-15, we studied the interaction of SBA-PA and SBA-SA with pyridine-^{15}N. The mass-to-mass ratios of pyridine and silica used in these studies are listed in Table 3. At room temperature, pyridine molecules adsorbed in mesoporous silica are involved in rapid exchange between different sites,[24] so that only a single weighted-average peak is present in the NMR spectra. This exchange was suppressed by performing low-temperature ^{15}N CPMAS NMR experiments at about 130 K. Typical results are shown in Figure 3. In all spectra the peak at 0 ppm corresponds to bulk frozen pyridine, and the peak at -25 ppm corresponds to pyridine hydrogen bonded to silanol groups of the silica surface.[24] The ^{15}N CPMAS NMR spectra of SBA-SA and SBA-PA exhibit a further broad peak at -109 and -100 ppm, respectively. The relative integrated intensities of the observed signals are listed in Table 3.

4. Discussion

The pure and functionalized SBA-15 materials were characterized by ^{29}Si MAS NMR, ^{13}C CPMAS NMR, and ^{1}H MAS NMR spectroscopy. ^{15}N CPMAS NMR at 130 K of samples loaded with pyridine-^{15}N was used to study the proton-donating ability of the functionalized materials. The main results of the experiments described above can be summarized as follows. The mole fraction of functional groups on the silica surface is about 25% for SBA-SA and 36% for SBA-PA. In contrast to pure SBA-15, the functionalized materials contain residual water which was not removed by evacuation at 420 K. Pyridine molecules adsorbed onto the silica materials form hydrogen-bonded complexes with surface silanol groups. The geometry of these complexes does not depend on surface functionalization. In addition, pyridine molecules adsorbed onto materials functionalized with sulfonic and phosphonic acid moieties form hydrogen-bonded ionic complexes with these functional groups. The geometry of the latter complexes depends on the type of the proton donor. In this section we present interpretations of these findings, which characterize the proton-donating ability of sulfonic ($R-SO_2OH$) and phosphonic ($R-PO(OH)_2$) groups at the surface of SBA-15 under almost water-free conditions.

4.1. Properties of Surface Silanol and Functional Groups. In our earlier work[24] we found that pyridine adsorbed onto SBA-15 silica that was calcined at 823 K forms hydrogen-bonded complexes with the protons of surface silanol groups. The isotropic ^{15}N chemical shift of these hydrogen-bonded pyridine molecules was -25 ppm relative to bulk pyridine. The same peak is also observed for the present SBA-15, SBA-SA, and SBA-PA materials, for which template removal was performed by treatment with sulfuric acid. According to eq 2, the bond order of H−N in these hydrogen bonds is $p_{HN} \approx 0.20$, corresponding to a distance $r_{HN} \approx 1.67$ Å (eq 1), and thus $p_{OH} \approx 0.80$, corresponding to a distance $r_{OH} \approx 1.03$ Å. Accordingly, from eq 3 one finds that the proton-donating ability of the surface silanol groups is equivalent to that of acids exhibiting in water a pK_a of about 5. For SBA-SA one also observes a peak at -109 ppm (Figure 3b). This peak is attributed to pyridine interacting with the sulfonic acid moiety on the surface. Using the same relations as above for this complex, one obtains $r_{HN} \approx 1.05$ Å, $r_{OH} \approx 1.69$ Å, and p$K_a \approx 0.6$. For SBA-PA interacting with pyridine a similar peak is found -100 ppm (Figure 3c). The respective parameters for the hydrogen bond in this complex are $r_{HN} \approx 1.09$ Å, $r_{OH} \approx 1.53$ Å, and $pK_a \approx 1.3$.

The density of the surface silanol groups in SBA-15 materials calcined at 823 K is about 3.7 nm^{-2}.[24] As mentioned above, none of the materials used in this work was calcined but treated with 48% aqueous H_2SO_4 for template removal, to avoid thermal decomposition of functional groups at the silica surface. The data collected in Tables 1 and 3, namely, the surface area and the pyridine-to-silica mass ratio, are sufficient to estimate the amount of pyridine loaded per unit area of the host material. The integrated intensities of the low-temperature ^{15}N CPMAS NMR signals correspond to the amount of pyridine in different states (Table 3). Of central interest are the amounts of pyridine hydrogen bonded to the silanol groups and the functional groups. The former is a direct measure of the density of surface silanol groups. For the pure SBA-15 material, this density is about 5.2 nm^{-2}, i.e., considerably higher than the value 3.7 nm^{-2} found for calcined SBA-15.[24] This finding supports the expectation that calcination results in a self-condensation of neighboring silanols and thus in a reduction of the number of silanol groups. Incidentally, the higher density of silanol groups on noncalcined silica is also qualitatively seen by ^{29}Si NMR. While for the calcined SBA-15 the Q^3:Q^4 ratio is about 1:4, this ratio is about 1:2.5 for the present H_2SO_4 treated sample.

TABLE 3: Relative Integrated Intensities of Low-Temperature ^{15}N CPMAS NMR Signals of SBA-15, SBA-SA, and SBA-PA Materials Loaded with Pyridine-^{15}N and the Corresponding Estimated Average Numbers of Different Chemically Active Groups on Their Inner Surfaces[a]

sample	Pyr/SBA	bulk Pyr	SiOH−Pyr	A^-−[H−Pyr]$^+$	$N_{OH}^{silanol}$ per nm^2	N_{OH}^{acid} per nm^2	$N_{OH}^{acid}/N_{OH}^{silanol}$
SBA-15	0.65	1.16	8.52	–	5.2	–	–
SBA-SA	0.30	1.44	3.85	1.27	2.3	0.8	0.35
SBA-PA	0.42	1.32	1.66	2.06	2.0	2.4	1.20

[a] Pyr/SBA, mass-to-mass ratio of pyridine-^{15}N loaded into silica samples after water removal; bulk Pyr, free pyridine (not involved in hydrogen bonding); SiOH−Pyr, pyridine hydrogen bonded to surface silanol groups; A^-−[H−Pyr]$^+$, pyridine hydrogen bonded to surface acidic groups; $N_{OH}^{silanol}$, number of accessible surface silanol hydroxyl groups; N_{OH}^{acid}, number of accessible surface sulfonic or phosphonic acid hydroxyl groups.

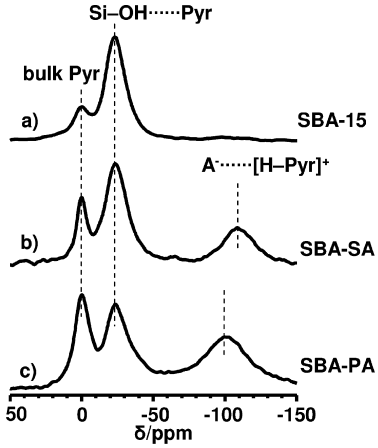

Figure 3. Solid-state ^{15}N CPMAS NMR spectra at 130 K of different silica samples loaded with pyridine-^{15}N: (a) SBA-15; (b) SBA-SA; (c) SBA-PA.

SBA-SA contains on average 2.3 silanol groups per nm^2 and in addition surface sulfonic acid moieties. Since each of these moieties can form one hydrogen bond with pyridine, the density of the sulfonic acid groups is equal to the density of the pyridine molecules resonating at −109 ppm, which was estimated to 0.8 species per nm^2 (Table 3). Hence the ratio of functional groups and silanol groups, $N_{OH}^{acid}/N_{OH}^{silanol}$, is about 0.35 in SBA-SA (Table 3). In Table 2 this ratio is estimated from the ^{29}Si NMR results, using the relation $N_{OH}^{acid}/N_{OH}^{silanol} = (T^3 + T^2)/(Q^3 + T^2) = 0.29$. However, it is not clear whether guest molecules can interact with the residual silanol groups of the T^2 species. Specifically, these silanol groups may be not accessible for pyridine due to steric hindrance. In this case an "effective" ratio of acid groups and silanol groups should be estimated by the relation $N_{OH}^{acid}/N_{OH}^{silanol} = (T^3 + T^2)/Q^3 = 0.33$. This value is closer to the one obtained from ^{15}N NMR than the former value. We interpret this trend as an indication of restricted accessibility of the residual silanol groups of T^2 species for guests. This finding agrees with our earlier observations.[25]

SBA-PA silica contains on average 2.0 surface silanol groups per nm^2 and the phosphonic acid moieties. Each of these moieties can form two hydrogen bonds. The density of the pyridine molecules resonating at −100 ppm is 2.4 per nm^2. Accordingly, the ratio $N_{OH}^{acid}/N_{OH}^{silanol}$ estimated from the ^{15}N NMR spectrum is 1.20 for SBA-PA (Table 3). From the ^{29}Si NMR spectrum, one finds $N_{OH}^{acid}/N_{OH}^{silanol} = T^3/Q^3 = 0.57$ when assuming that each moiety interacts with only one pyridine, or $N_{OH}^{acid}/N_{OH}^{silanol} = (2 \cdot T^3)/Q^3 = 1.14$ when assuming interactions with two pyridine molecules (Table 2). Hence a comparison with the value resulting from ^{15}N NMR strongly suggests that each phosphonic acid moiety can form two equal hydrogen bonds with two pyridine molecules.

We emphasize that while the ^{29}Si NMR experiment gives the $N_{OH}^{acid}/N_{OH}^{silanol}$ ratio directly, the estimate based on ^{15}N NMR is indirect, using properties of guest molecules. From the fact that the results obtained by the two methods are in reasonable agreement for both functionalized SBA-15 materials, we conclude that both methods independently and correctly estimate the relative amount of different chemically active groups on silica surfaces. On this basis the discussion can be taken a step further to learn more about the morphology of the SBA-15, SBA-SA, and SBA-PA samples. For clarity we introduce the following notation: The surface density of the different species is denoted as S_m^g, where m = cal, chem, SA, PA and g = silanol, acid. Here, cal stands for the SBA-15 material calcined at 823 K studied earlier (see refs 24 and 25), chem denotes chemical polymer removal (using 48% H_2SO_4), i.e., the pure SBA-15 sample studied in this work, and SA and PA stand for SBA-SA and SBA-PA, respectively. The indices silanol and acid indicate the surface silanol and functional groups, as above. For pure SBA-15 calcined at 823 K, we have $S_{cal}^{silanol} = 3.7$ nm^{-2} and $Q_{cal}^3/Q_{cal}^4 = 0.25$ from our earlier study,[24,25] while for the present sample with chemical template removal we find $S_{chem}^{silanol} = 5.2$ nm^{-2} and $Q_{chem}^3/Q_{chem}^4 = 0.4$. At first sight, this result is unexpected since the specific surface areas of these two materials are similar (ca. 800 m^2 g^{-1}; see Table 1 and refs 24 and 25). As a first approximation we infer that the only effect of calcination is a partial condensation of Q^3 groups to Q^4 groups. In this case one expects $Q_{cal}^3 + Q_{cal}^4 = Q_{chem}^3 + Q_{chem}^4$. By inserting the above relations for Q^3/Q^4 of the two materials this leads to $Q_{chem}^3/Q_{cal}^3 = 1.43$, based on the ^{29}Si NMR data. The corresponding ratio based on the ^{15}N NMR data is $S_{chem}^{silanol}/S_{cal}^{silanol} = 1.41$. From the fact that the two values are nearly the same, i.e., $S_{chem}^{silanol}/S_{cal}^{silanol} \approx Q_{chem}^3/Q_{cal}^3$, we conclude that almost all silanol groups on pure SBA-15 are accessible for pyridine molecules.

For the functionalized materials, when assuming that the functional groups at the surface are replacing silanol groups, the ratio Q_{chem}^3/Q_{chem}^4 of the pure silanol is to be compared with the ratios $(Q_{SA}^3 + T_{SA}^2 + T_{SA}^3)/Q_{SA}^4 = 0.56$ for SBA-SA, and $(Q_{PA}^3 + T_{PA}^3)/Q_{PA}^4 = 0.58$ for SBA-PA (see Table 2). The higher values of these ratios compared to Q_{chem}^3/Q_{chem}^4 might be taken as an indication for an increase of the surface roughness upon functionalization. However, this conclusion is inconsistent with the fact that the functionalized materials have lower specific surface areas than pure SBA-15 prepared under similar conditions, i.e., $(a_s)_{SA}/(a_s)_{chem} \approx (a_s)_{PA}/(a_s)_{chem} \approx 0.7$ (Table 1). Moreover, the density of the chemically active surface groups is remarkably reduced. For SBA-SA and SBA-PA this is seen by comparing the values $S_{SA}^{silanol} + S_{SA}^{acid} = 3.1$ nm^{-2} and $S_{PA}^{silanol} + S_{PA}^{acid} = 3.2$ nm^{-2} with $S_{chem}^{silanol} = 5.2$ nm^{-2}. To solve this puzzle it must be remembered that in SBA-SA and SBA-PA the functional groups have not been grafted onto the surface but incorporated by co-condensation of the functional silane with the silica precursor. If it is inferred that functional groups have been formed at the expense of Q^4 species, then the ratio Q_{chem}^3/Q_{chem}^4 of the pure silanol is to be compared with the ratios $Q_{SA}^3/$

SCHEME 2: Schematic Representation of Geometrical Parameters of Hydrogen-Bonded Complexes Formed between Chemically Active Surface Groups of (a) SBA-SA and (b) SBA-PA and Pyridine at 130 K

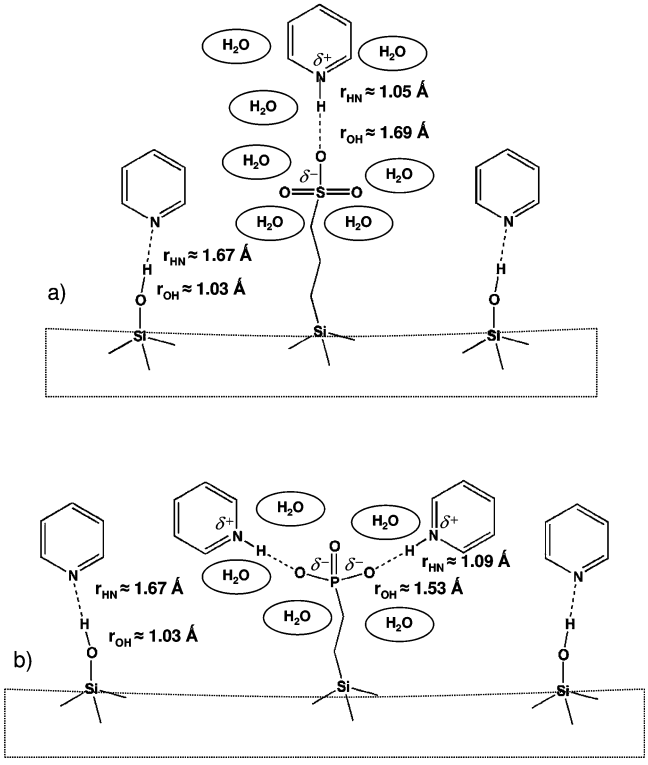

$(Q^4_{SA} + T^2_{SA} + T^3_{SA}) = 0.38$ for SBA-SA and $Q^3_{PA}/(Q^4_{PA} + T^3_{PA}) = 0.30$ for SBA-PA. These values are lower than the value $Q^3_{chem}/Q^4_{chem} = 0.4$ for pure SBA-15, but closer to that value than those expected on the basis of a replacement of silanol groups. In this context it is worth mentioning that MCM-41 silica, having rather smooth pore walls, is characterized by $S^{silanol}_{MCM-41} = 3$ nm^{-2} and $Q^3_{MCM-41}/Q^4_{MCM-41} = 0.3$.[25] We do not have enough data to claim that the pore wall structures of the SBA-SA and SBA-PA materials are similar to the structure of MCM-41. Nevertheless, the similar values may indicate that the functionalization of SBA-15 causes a smoothing of the pore walls. However, this smoothing should have a different nature than achieved by postsynthesis alumination of SBA-15.[52] The latter process should probably lead to blocking of micropores penetrating the interpore walls of SBA-15 and result in the appearance of silanol groups nonaccessible for guest molecules.

4.2. Mechanism of the Formation of Hydrogen-Bonded Complexes with Proton Transfer on Functionalized Silica Surfaces. The discussion above can be summarized as follows: (i) each sulfonic acid moiety in SBA-SA interacts with one pyridine molecule; (ii) each phosphonic acid moiety in SBA-PA interacts simultaneously with two pyridine molecules; (iii) for both materials the interaction of the acid moieties with pyridine results in proton transfer to pyridine. The conclusions (i) and (ii) indicate that the functional groups do not interact with each other in the presence of pyridine. Thus, mutual interactions cannot be the reason for the observed proton transfer. In aqueous solution the pK_a of methylsulfonic acid is -0.6, and the pK_a of ethylphosphonic acid is 2.4 for the first proton and 7.8 for the second proton.[53,54] Our data also correlate with a higher acidity of the sulfonic acid moieties. The N···H distance in their complexes with pyridine is 1.05 Å for sulfonic acid and 1.09 Å for phosphonic acid moieties. Concerning the deprotonation states of phosphonic acid, one should distinguish between solvated ions in the aqueous solution, where the phosphonic acid anion can be singly or doubly charged, and a zwitterionic complex with phosphonic acid. This zwitterionic complex is a dipole, and its geometry depends on the local electric field or properties of a hydrogen bond network.

Therefore, our current question is what is the driving force for the proton transfer in the zwitterionic complexes formed between the surface acid groups and adsorbed pyridine. To answer this question, we analyze the ^{1}H spectra shown in Figure 2 in more detail. We especially concentrate our attention on the spectrum of SBA-SA evacuated at 420 K (Figure 2d). This spectrum contains two resolved peaks centered at 1.8 and 6.5 ppm. The ratio of their integrated intensities is about 2:3. We remember that SBA-SA contains on average 2.3 residual silanol groups and 0.8 propylsulfonic acid moieties per nm^2. Each moiety contributes six alkyl protons and one hydroxyl proton in the integrated intensity. The alkyl protons should resonate close to 2 ppm. The chemical shifts of the protons of Si−OH and R−SO_2OH groups depend on their bonding situation, i.e., whether they are involved in hydrogen bonds or not. In the latter case they also would resonate near 2 ppm. The presence of the peak at 6.5 ppm is evidence that at least some of these hydroxyl groups are involved in hydrogen bonds. The ratio of the integrated intensities of the peaks in Figure 2d indicates that the amount of protons in the hydrogen-bonded phase is much higher than the amount of the hydroxyl groups. Therefore, we conclude that SBA-SA contains residual water after evacuation at 420 K. Since pure SBA-15 does not contain water after such treatment, we may infer that the residual water is somehow structured around the sulfonic acid groups. These solvated sulfonic acid species resonate at 6.5 ppm. In contrast, the surface silanol groups are spatially separated from these species and resonate close to 2 ppm. In order to satisfy the experimentally observed ratio of the integrated intensities, SBA-SA must contain about five water molecules per nm^2, which is equal to six water molecules per each sulfonic acid moiety. Residual water must also be responsible for the proton transfer in the complexes of phosphonic acid moieties with pyridine, but the quality of the corresponding spectrum is insufficient for a quantitative estimate of the number of water molecules in the complex with phosphonic acid.

5. Conclusions

It has been demonstrated that a combination of various solid-state NMR techniques makes it possible to describe chemical and structural properties of surface-functionalized mesoporous SBA-15 materials. In particular, the surface density of the functional groups, their accessibility for guests molecules, and an "effective" chemical reactivity of this groups have been evaluated. We speak here about the effective chemical reactivity of the functional groups since their chemical properties are affected by residual water which cannot be easily removed from silica samples.

In this work we have compared pure SBA-15 with samples of sulfonic acid-functionalized SBA-15 (SBA-SA) and phosphonic acid-functionalized SBA-15 (SBA-PA) synthesized by the co-condensation method. All three materials were prepared in a similar way (template removal by treatment with sulfuric acid). The density of silanol groups on the surface of the pure SBA-15 is 5.2 nm^{-2}, i.e. significantly higher than in SBA-15 calcined at 823 K, where it is 3.7 nm^{-2}. In the functionalized materials, the surface density of silanol and acid moieties is 2.3 and 0.8 nm^{-2} (SBA-SA), and 2.0 and 1.2 nm^{-2} (SBA-PA),

respectively. It is shown that all acid moieties are accessible for pyridine molecules. At 130 K each sulfonic acid moiety in SBA-SA interacts with one pyridine molecule, and each phosphonic acid moiety in SBA-PA interacts simultaneously with two pyridine molecules. For both materials the interaction of the acid moieties with pyridine results in proton transfer to pyridine. This effect is attributed to the presence of residual water in SBA-SA and SBA-PA. Whereas all water can be removed from pure SBA-15 by evacuation at 420 K, the SBA-SA material after the same treatment contains about five residual water molecules per nm^2. This water is arranged around the hydrophilic heads of the functional moieties and affects their proton-donating ability. In this small water-cluster environment, the proton-donating abilities of the hydroxyl group of sulfonic acid, and the two hydroxyl groups of phosphonic acid, are equivalent to the proton-donating ability of acids exhibiting in water pK_a values of about 0.6 and 1.3, respectively. Host−guest interactions at the surface of pure SBA-15 and the two acid-functionalized SBA-15 materials are indicated schematically in Scheme 2. In this scheme geometrical parameters of the hydrogen-bonded complexes formed between the chemically active surface groups of the hosts and pyridine at 130 K are shown.

Acknowledgment. This work was supported by the Deutsche Forschungsgemeinschaft in the framework of SFB 448 "Mesoscopically Organized Composites" and SONS-AMPHI (Project FI 235/16), the Russian Ministry of Education and Science (Project RNP 2.1.1.485), and the Russian Foundation of Basic Research (Project 09-03-91336-NNIO_a).

Supporting Information Available: Characterization of pure and acid-functionalized SBA-15 by N_2 adsorption, SAXD, and SEM. Characterization of acid-functionalized SBA-15 by solid-state ^{13}C CPMAS NMR. This information is available free of charge via the Internet at http://pubs.acs.org.

References and Notes

(1) Goodwin, E. J.; Howard, N. W.; Legon, A. C. *Chem. Phys. Lett.* **1986**, *131*, 319–324.
(2) Howard, N. W.; Legon, A. C. *J. Chem. Phys.* **1988**, *88*, 4694–4701.
(3) Latajka, Z.; Sakai, S.; Morokuma, K.; Ratajczak, H. *Chem. Phys. Lett.* **1984**, *110*, 464–468.
(4) Cazar, R.; Jamka, A.; Tao, F.-M. *Chem. Phys. Lett.* **1998**, *287*, 549–552.
(5) Jordan, M. J. T.; Del Bene, J. E. *J. Am. Chem. Soc.* **2000**, *122*, 2101–2115.
(6) Bacelo, D. E.; Fioressi, S. E. *J. Chem. Phys.* **2003**, *119*, 11695–11703.
(7) Barnes, A. J.; Beech, T. R.; Mielke, Z. *J. Chem. Soc., Faraday Trans.* **1984**, *80*, 455–463.
(8) Golubev, N. S.; Shenderovich, I. G.; Smirnov, S. N.; Denisov, G. S.; Limbach, H.-H. *Chem.—Eur. J.* **1999**, *5*, 455492–497.
(9) Shenderovich, I. G.; Burtsev, A. P.; Denisov, G. S.; Golubev, N. S.; Limbach, H.-H. *Magn. Reson. Chem.* **2001**, *39*, S91–S99.
(10) Chapman, K.; Crittenden, D.; Bevitt, J.; Jordan, M. J. T.; Del Bene, J. E. *J. Phys. Chem.* **2001**, *105*, 5442–5449.
(11) Del Bene, J. E.; Jordan, M. J. T. *J. Mol. Struct. (THEOCHEM)* **2001**, *573*, 11–23.
(12) Glezakou, V. A.; Dupuis, M.; Mundy, C. J. *Phys. Chem. Chem. Phys.* **2007**, *9*, 5752–5760.
(13) Jiang, F.; Kaltbeitzel, A.; Fassbender, B.; Brunklaus, G.; Pu, H.; Meyer, W. H.; Spiess, H. W.; Wegner, G. *Macromol. Chem. Phys.* **2008**, *209*, 2494–2503.
(14) Dos, A.; Schimming, V.; Limbach, H.-H. *J. Phys. Chem. B* **2008**, *112*, 15604–15615.
(15) Manriquez, R.; Lopez-Dellamary, F. A.; Frydel, J.; Emmler, T.; Breitzke, H.; Buntkowsky, G.; Limbach, H.-H.; Shenderovich, I. G. *J. Phys. Chem. B* **2009**, *113*, 934–940.
(16) Corma, A. *Chem. Rev.* **1995**, *95*, 559–614.
(17) Taguchi, A.; Schüth, F. *Microporous Mesoporous Mater.* **2004**, *77*, 1–45.
(18) Renard, G.; Mureseanu, M.; Galarneau, A.; Lerner, D. A.; Brunel, D. *New J. Chem.* **2005**, *29*, 912–918.
(19) Kim, D. J.; Dunn, B. C.; Huggins, F.; Huffman, G. P.; Kang, M.; Yie, J. E.; Eyring, E. M. *Energy Fuels* **2006**, *20*, 2608–2611.
(20) Galarneau, A.; Iapichella, J.; Bonhomme, K.; Di Renzo, F.; Kooyman, P.; Terasaki, O.; Fajula, F. *Adv. Funct. Mater.* **2006**, *16*, 1657–1667.
(21) Akcakayiran, D.; Mauder, D.; Hess, C.; Sievers, T. K.; Kurth, D. G.; Shenderovich, I.; Limbach, H.-H.; Findenegg, G. H. *J. Phys. Chem. B* **2008**, *112*, 14637–14647.
(22) Hayward, R. C.; Alberius-Henning, P.; Chmelka, B. F.; Stucky, G. D. *Microporous Mesoporous Mater.* **2001**, *44*, 619–624.
(23) Juarez, R.; Padilla, A.; Corma, A.; Garcia, H. *Cat. Comm.* **2009**, *10*, 472–476.
(24) Shenderovich, I. G.; Buntkowsky, G.; Schreiber, A.; Gedat, E.; Sharif, S.; Albrecht, J.; Golubev, N. S.; Findenegg, G. H.; Limbach, H.-H. *J. Phys. Chem. B* **2003**, *107*, 11924–11939.
(25) Shenderovich, I. G.; Mauder, D.; Akcakayiran, D.; Buntkowsky, G.; Limbach, H.-H.; Findenegg, G. H. *J. Phys. Chem. B* **2007**, *111*, 12088–12096.
(26) Sharif, S.; Shenderovich, I. G.; Gonzalez, L.; Denisov, G. S.; Silverman, D. N.; Limbach, H.-H. *J. Phys. Chem. A* **2007**, *111*, 6084–6093.
(27) Stein, A.; Melde, B. J.; Schroden, R. C. *Adv. Mater.* **2000**, *12*, 1403–1419.
(28) Chong, A. S. M.; Zhao, X. S. *J. Phys. Chem. B* **2003**, *107*, 12650–12657.
(29) Hoffmann, F.; Cornelius, M.; Morell, J.; Froba, M. *Angew. Chem., Int. Ed.* **2006**, *45*, 3216–3251.
(30) Vallet-Regi, M.; Balas, F.; Arcos, D. *Angew. Chem., Int. Ed.* **2007**, *46*, 7548–7558.
(31) Garcia, N.; Benito, E.; Guzman, J.; Tiemblo, P.; Morales, V.; Garcia, R. A. *Mesoporous Microporous Mater.* **2007**, *106*, 129–139.
(32) Rosenholm, J. M.; Czuryszkiewicz, T.; Kleitz, F.; Rosenholm, J. B.; Linden, M. *Langmuir* **2007**, *23*, 4315–4323.
(33) Ispas, C.; Sokolov, I.; Andreescu, S. *Anal. Bioanal. Chem.* **2009**, *393*, 543–554.
(34) Mbaraka, I. K.; Shanks, B. H. *J. Catal.* **2006**, *244*, 78–85.
(35) Kanthasamy, R.; Mbaraka, I. K.; Shanks, B. H.; Larsen, S. C. *Appl. Magn. Reson.* **2007**, *32*, 513–526.
(36) Krishtal, A.; Senet, P.; Van Alsenoy, C. *J. Chem. Theory Comput.* **2008**, *4*, 2122–2129.
(37) Yang, C. M.; Wang, Y. Q.; Zibrowius, B.; Schüth, F. *Phys. Chem. Chem. Phys.* **2004**, *6*, 2461–2467.
(38) Schreiber, A.; Ketelsen, I.; Findenegg, G. H. *Phys. Chem. Chem. Phys.* **2001**, *3*, 1185–1195.
(39) Ravikovitch, P. I.; Neimark, A. V. *J. Phys. Chem. B* **2001**, *105*, 6817–6823.
(40) Jaroinec, M.; Solovyov, L. A. *Langmuir* **2006**, *22*, 6757–6760.
(41) Whaley, T. W.; Ott, D. G. *J. Labelled Compd.* **1974**, *10*, 283–286.
(42) Lorente, P.; Shenderovich, I. G.; Golubev, N. S.; Denisov, G. S.; Buntkowsky, G.; Limbach, H.-H. *Magn. Reson. Chem.* **2001**, *39*, S18–S29.
(43) Steiner, Th. *J. Phys. Chem. A.* **1998**, *102*, 7041–7052.
(44) Limbach, H.-H.; Pietrzak, M.; Sharif, S.; Tolstoy, P. M.; Shenderovich, I. G.; Smirnov, S. N.; Golubev, N. S.; Denisov, G. S. *Chem.—Eur. J.* **2004**, *10*, 5195–5204.
(45) Corriu, R. J. P.; Datas, L.; Guari, Y.; Mehdi, A.; Reye, C.; Thieuleux, C. *Chem. Commun.* **2001**, 763–764.
(46) Aliev, A.; Li Ou, D.; Ormsby, B.; Sullivan, A. C. *J. Mater. Chem.* **2000**, *10*, 2758–2764.
(47) Gruenberg, B.; Emmler, T.; Gedat, E.; Shenderovich, I.; Findenegg, G. H.; Limbach, H.-H.; Buntkowsky, G. *Chem.—Eur. J.* **2004**, *10*, 5689–5696.
(48) Pizzanelli, S.; Kababya, S.; Frydman, V.; Landau, M.; Vega, S. *J. Phys. Chem. B* **2005**, *109*, 8029–8039.
(49) Buntkowsky, G.; Breitzke, H.; Adamczyk, A.; Roelofs, F.; Emmler, T.; Gedat, E.; Grünberg, B.; Xu, Y.; Limbach, H.-H.; Shenderovich, I.; Vyalikh, A.; Findenegg, G. *Phys. Chem. Chem. Phys.* **2007**, *9*, 4843–4853.
(50) Margolese, D.; Melero, J. A.; Christiansen, S. C.; Chmelka, B. F.; Stucky, G. D. *Chem. Mater.* **2000**, *12*, 2448–2459.
(51) Morales, G.; Athens, G.; Chmelka, B. F.; van Grieken, R.; Melero, J. A. *J. Catal.* **2008**, *254*, 205–217.
(52) Zukal, A.; Siklova, H.; Cejka, J. *Langmuir* **2008**, *24*, 9837–9842.
(53) March, J. *Advanced Organic Chemistry*, third ed.; John Wiley & Sons: New York, 1985.
(54) Brown, H. C.; Daniel, D. H.; Häfliger, O. In *Determination of Organic Structures by Physical Methods*; Braude, E. A., Nachod, F. C., Eds.; Academic Press: New York, 1955.

JP907058Y